Soft x-ray absorption spectroscopy and magnetic circular dichroism study of the valence and spin states in spinel $MnFe_2O_4$

J.-S. Kang,[1,*] G. Kim,[1] H. J. Lee,[1] D. H. Kim,[1] H. S. Kim,[1] J. H. Shim,[2] S. Lee,[2] Hangil Lee,[3] J.-Y. Kim,[3] B. H. Kim,[4] and B. I. Min[4]

[1]*Department of Physics, The Catholic University of Korea, Bucheon 420-743, Korea*

[2]*Department of Physics, Korea Advanced Institute of Science and Technology, Daejeon 305-701, Korea*

[3]*Pohang Accelerator Laboratory (PAL), POSTECH, Pohang 790-784, Korea*

[4]*Department of Physics, POSTECH, Pohang 790-784, Korea*

(Received 23 July 2007; published 17 January 2008)

The valence and spin states of $MnFe_2O_4$ spinel oxide have been investigated by employing soft x-ray absorption spectroscopy (XAS) and x-ray magnetic circular dichroism (XMCD). The measured Mn $2p$ and Fe $2p$ XAS spectra indicate that Mn and Fe ions are nearly divalent (Mn^{2+}) and trivalent (Fe^{3+}), respectively. Our XAS and XMCD spectra for $MnFe_2O_4$ do not show clear evidence of mixed-valent states but provide evidence for the inversion of both Mn and Fe ions, with $T_d/O_h \sim 0.8/0.2$ for Mn ions and $T_d/O_h \sim 0.1/0.9$ for Fe ions, respectively. Based on our data, $MnFe_2O_4$ can be described either by the single-valence states of $(Mn^{2+}_{0.8}Fe^{3+}_{0.2})_A[Fe^{3+}_{1.8}Mn^{2+}_{0.2}]_BO_4$ or by the mixed-valence states of $(Mn^{2+}_{0.8}Fe^{3+}_{0.2})_A[Fe^{3+}_{1.6}Fe^{2+}_{0.2}Mn^{3+}_{0.2}]_BO_4$.

DOI: 10.1103/PhysRevB.77.035121 PACS number(s): 78.70.Dm, 87.64.K−, 75.50.Gg, 74.25.Jb

The AB_2O_4-type spinel oxides, which are the most abundant structures on earth, have attracted renewed attention because of their possible application as new functional materials as well as many interesting phenomena observed, such as Jahn-Teller (JT) effects and phase separations.[1] In AB_2O_4 spinels, a cation occupies either the tetrahedral (T_d) A site or the octahedral (O_h) B site. When both A and B ions are magnetic ions, such as in Fe_3O_4, a ferrimagnetic ordering is often observed since the main A-B interaction is antiferromagnetic (AFM).[2] $MnFe_2O_4$ is one of the well-known ferrimagnetic spinel oxides with a partially inverted spinel structure described by the formula $(Mn_{1-y}Fe_y)_A[Fe_{2-y}Mn_y]_BO_4$, where y is called the inversion parameter. The inversion parameter is known to vary from 0 to 0.2 depending on the ways of thermal treatment, among which 0.2 is the most usual.[3] If all the Mn ions are divalent (Mn^{2+}) and all the Fe ions are trivalent (Fe^{3+}), then the magnetic moment is expected to be $5\mu_B$/f.u. in the ionic model. From magnetic scattering measurements,[3] the magnetic moment of $MnFe_2O_4$ was found to be $\sim 4.6\mu_B$/f.u. This reduced magnetic moment of $MnFe_2O_4$ has drawn much attention.[4]

There have been several models that explain the reduced magnetic moment of $MnFe_2O_4$. Harrison *et al.*[5] proposed the mixed valency for Mn and Fe ions such that some of Mn ions are trivalent (Mn^{3+}) and that some of Fe ions are divalent (Fe^{2+}), assuming the collinear ferrimagnetic spin order between Mn^{3+} and Fe^{2+} pairs in B sites. The structural formula in this case was assumed to be $(Mn^{2+}_{1-y}Fe^{3+}_y)_A[Fe^{3+}_{2-2y}Fe^{2+}_yMn^{3+}_y]_BO_4$. On the other hand, Mössbauer measurements of $MnFe_2O_4$ revealed little Fe^{2+} ions in B sites, and so the canted ferrimagnetic spin order was proposed.[6] The canted spin structure was supported by the $M(T)$ curve.[7] However, nuclear magnetic resonance (NMR) experiments showed no evidence of spin canting.[8,9] Based on recent NMR measurements, some of the authors of this work[10] reported the existence of Fe^{3+} ions in A sites and Mn^{3+} and Fe^{2+} ions in B sites. Then, in order to explain the reduced magnetic moment, an AFM order among Fe spins in B sites was proposed in addition to the AFM order between Fe spins in A and B sites. Hence, the above models are controversial to one another, and the valence states and the spin ordering in $MnFe_2O_4$ are still open issues.

Therefore, it is important to determine the valence states of Mn and Fe ions in $MnFe_2O_4$ and their distribution between $T_d(A)$ and $O_h(B)$ sites more precisely. Soft x-ray absorption spectroscopy[11–13] (XAS) and soft x-ray magnetic circular dichroism[14,15] (XMCD) are powerful experimental tools for studying the valence and spin states of transition-metal (T) ions in solids and the element-specific local magnetic moments of spin (m_s) and orbital (m_l) components, respectively. In both XAS and XMCD, photons at specific characteristic energies are absorbed to produce the transition of a core electron to an empty state above the Fermi level, which is governed by the dipole selection rules. T $2p$ XAS and XMCD spectra of transition-metal oxides often show the multiplet structures, and their line shapes are strongly dependent on the occupied $3d$ electron configurations, the crystal field, the spin-orbit and electron-electron interactions within the T atom, and the hybridization of $3d$ electrons to other valence electrons.

We have investigated the electronic structures of $MnFe_2O_4$ by employing XAS and XMCD. We have determined the valence and spin states of Mn and Fe ions and the amount of the inverted structure. This is the first XMCD study on *bulk* stoichiometric $MnFe_2O_4$. As to the related spinel oxides, the XMCD study has been reported for $Zn_{1/3}Mn_{2/3}Fe_2O_4$ (Ref. 16) and nanocrystalline thin films of $Mn_xFe_{3-x}O_4$.[17]

The $MnFe_2O_4$ sample used in this study is a commercially available polycrystalline powder of 99.9% purity synthesized by KOJUNDO Chemical. Scanning electron microscope measurements showed that the sizes of samples are larger than a few micrometers. X-ray powder diffraction measurements also showed the sharp peaks that are characteristic of the single-phase bulk spinel structure.[18] XAS and XMCD experiments were performed at the 2A EPU beamline of the

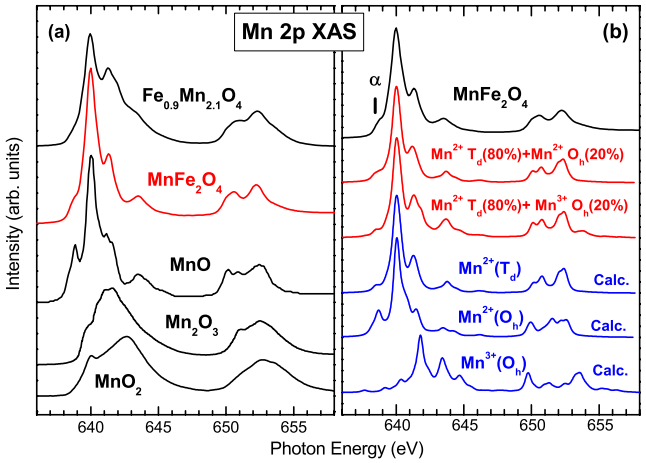

FIG. 1. (Color online) (a) Comparison of the Mn $2p$ XAS of $MnFe_2O_4$ to those of $Fe_{0.9}Mn_{2.1}O_4$ and the reference Mn oxides, such as MnO (Mn^{2+}) (Ref. 21), Mn_2O_3 (Mn^{3+}) (Ref. 22), and MnO_2 (Mn^{4+}) (Ref. 21). (b) Comparison of the Mn $2p$ XAS of $MnFe_2O_4$ to the calculated Mn $2p$ XAS for T_d Mn^{2+}, O_h Mn^{2+}, and O_h Mn^{3+} ions and their weighted sums (red lines).

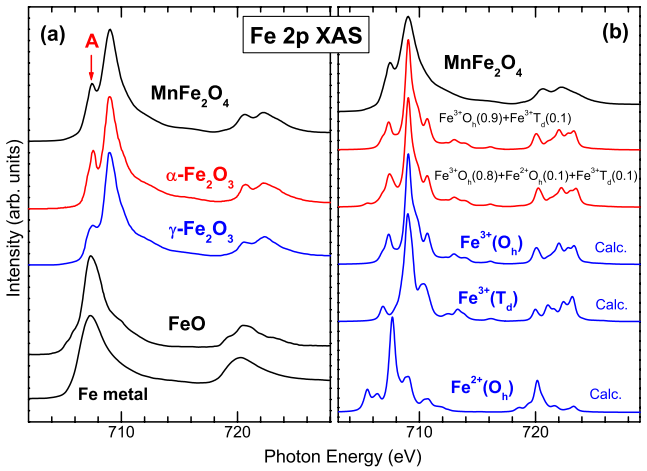

FIG. 2. (Color online) (a) Comparison of the Fe $2p$ XAS of $MnFe_2O_4$ to those of α-Fe_2O_3 (Ref. 24), γ-Fe_2O_3 (Ref. 23), FeO (Ref. 24), and Fe metal (Ref. 25). (b) Comparison of the Fe $2p$ XAS of $MnFe_2O_4$ to the calculated Fe $2p$ XAS for O_h Fe^{3+}, T_d Fe^{3+}, and O_h Fe^{2+} ions and their weighted sums (red lines).

PAL by using the circularly polarized light with the degree of circular polarization >90%. The XAS and XMCD data were collected in the total electron yield (TEY) mode.[19] The XMCD spectra were taken for a fixed helicity of light by reversing the applied magnetic field (~0.7 T) at each $h\nu$. The base pressure of the system was $\sim 5\times 10^{-10}$ Torr. All the data were obtained at $T\sim 80$ K. The total resolution for XAS was less than 100 meV, while that for XMCD was ~120 meV at the Mn $2p$ and Fe $2p$ edges.

Figure 1(a) compares the measured Mn $2p$ XAS spectrum of $MnFe_2O_4$ to those of $Fe_{0.9}Mn_{2.1}O_4$ single crystal[20] and the reference Mn oxides of MnO (Mn^{2+}),[21] Mn_2O_3,[22] and MnO_2 (Mn^{3+}).[21] The Mn $2p$ XAS spectrum of $MnFe_2O_4$ is qualitatively similar to that of MnO but quite different from those of Mn_2O_3 and MnO_2, suggesting that Mn ions in $MnFe_2O_4$ are nearly divalent. In contrast, the line shape of $Fe_{0.9}Mn_{2.1}O_4$ is rather different from that of $MnFe_2O_4$, which appears to be a mixture of MnO and Mn_2O_3, indicating the Mn^{2+}-Mn^{3+} mixed-valent states in $Fe_{0.9}Mn_{2.1}O_4$. This comparison reveals clearly that Mn ions in $MnFe_2O_4$ are nearly divalent, while Mn ions in $Fe_{0.9}Mn_{2.1}O_4$ are mixed valent.

To confirm this argument, we have compared the Mn $2p$ XAS spectrum of $MnFe_2O_4$ to the calculated Mn $2p$ XAS spectra in Fig. 1(b). The calculated spectra were obtained by employing the ligand-field multiplet (LFM) model[11,12] by including the spin-orbit interaction between $3d$ electrons. The three calculated XAS spectra (blue lines) represent those for $Mn^{2+}(3d^5)$ under the T_d symmetry, $Mn^{2+}(3d^5)$ under the O_h symmetry, and $Mn^{3+}(3d^4)$ under the O_h symmetry, with the crystal field energy $10Dq$=0.6 eV, $10Dq$=1.2 eV, and $10Dq$=1.2 eV, respectively. The two red curves represent the weighted sums of [80% $Mn_A^{2+}(T_d)$ and 20% $Mn_B^{2+}(O_h)$] to describe the single-valence states of Mn ions and [80% $Mn_A^{2+}(T_d)$ and 20% $Mn_B^{3+}(O_h)$] to describe the mixed-valence states of Mn ions. In Fig. 1(b), it is seen that the fitting with the single-valent Mn ions seems to be slightly better than that with the mixed-valent Mn ions, in particular, for the feature α around $h\nu\sim 639$ eV. However, considering the uncertainties in fitting, both fits should be considered to be good. Hence, at the moment, we cannot finalize whether $MnFe_2O_4$ is $(Mn_{0.8}^{2+}Fe_{0.2}^{3+})_A[Fe_{1.8}^{3+}Mn_{0.2}^{2+}]_BO_4$ or $(Mn_{0.8}^{2+}Fe_{0.2}^{3+})_A[Fe_{1.6}^{3+}Fe_{0.2}^{2+}Mn_{0.2}^{3+}]_BO_4$. In both cases, the inversion parameter $y\approx 0.2$ gives the best fitting for Mn $2p$ XAS of $MnFe_2O_4$.

Figure 2(a) shows the measured Fe $2p$ XAS spectrum of $MnFe_2O_4$. As a guide of the valence states of Fe ions, it is compared to those of α-Fe_2O_3 (Refs. 23,24) and γ-Fe_2O_3 (Refs. 23) both as formally trivalent Fe^{3+} oxides ($3d^5$) but having different local symmetries, FeO (Ref. 24) as a formally divalent Fe^{2+} oxide ($3d^6$), and Fe metal.[25] The line shape of the Fe $2p$ XAS spectrum of $MnFe_2O_4$ is very similar to those of both α-Fe_2O_3 and γ-Fe_2O_3 but quite different from those of FeO and Fe metal, indicating that the valence states of Fe ions in $MnFe_2O_4$ are mainly trivalent (3+). The minor difference in the feature "A" for $MnFe_2O_4$ from those for α-Fe_2O_3 and γ-Fe_2O_3 seems to indicate that Fe ions in $MnFe_2O_4$ occupy not only $B(O_h)$ sites but also $A(T_d)$ sites. This is because Fe^{3+} ions in α-Fe_2O_3 are located only at O_h sites, whereas Fe^{3+} ions in γ-Fe_2O_3 are at both T_d and O_h sites.[28] A similar trend has been observed in the calculated XAS for $Fe_B^{3+}(O_h)$ and $Fe_A^{3+}(T_d)$ ions.[26–28] This argument is also supported in Fig. 4.

In Fig. 2(b), we have compared the measured Fe $2p$ XAS spectrum of $MnFe_2O_4$ to the calculated Fe $2p$ XAS spectra, obtained from the LFM calculations. The three calculated XAS spectra (blue lines) represent those for $Fe^{3+}(3d^5)$ under O_h with $10Dq$=1.5 eV, $Fe^{3+}(3d^5)$ under T_d with $10Dq$ =1.2 eV, and $Fe^{2+}(3d^6)$ under O_h with $10Dq$=1.5 eV. The two red curves represent the weighted sums of [90% $Fe_B^{3+}(O_h)$ and 10% $Fe_A^{3+}(T_d)$] to describe the single-valence states of Fe ions and [80% $Fe_B^{3+}(O_h)$, 10% $Fe_B^{2+}(O_h)$, and 10% $Fe_A^{3+}(T_d)$] to describe the mixed-valence states of Fe

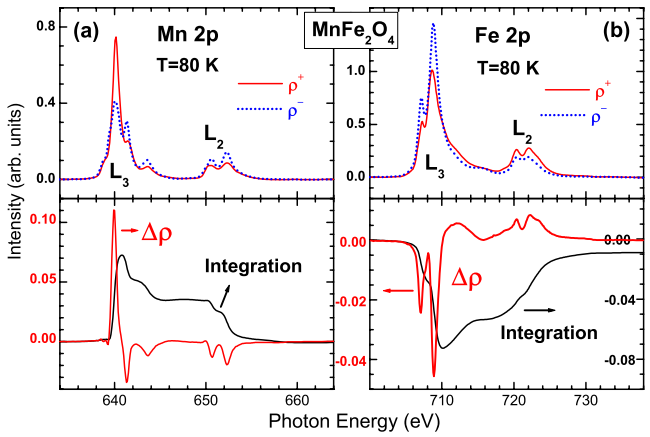

FIG. 3. (Color online) (a) The Mn $2p$ XAS spectra of $MnFe_2O_4$, obtained with different photon helicities (ρ_+ and ρ_-), the Mn $2p$ XMCD spectrum (red) ($\Delta\rho=\rho_+-\rho_-$), and its integrated value (black). (b) Similarly for the Fe $2p$ states.

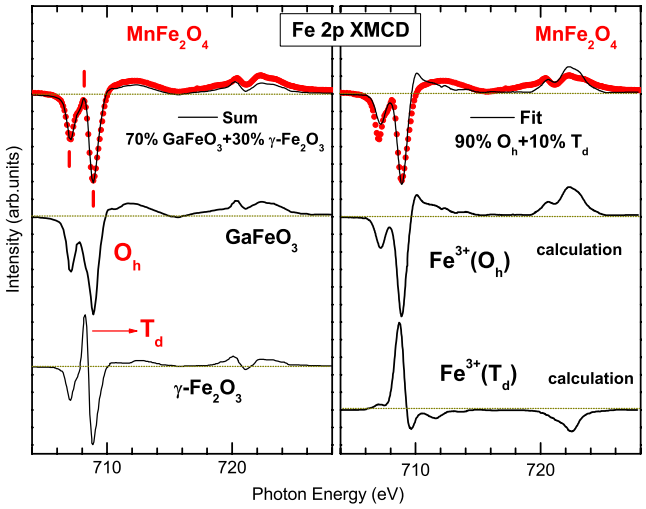

FIG. 4. (Color online) Comparison of the Fe $2p$ XMCD spectrum of $MnFe_2O_4$ to those of γ-Fe_2O_3 (Ref. 28) and $GaFeO_3$ (Ref. 23) (left) and their weighted sum (left) and to those of the calculated Fe $2p$ XMCD spectra for Fe_B^{3+} (O_h) (Ref. 28) and Fe_A^{3+} (T_d) (Ref. 28) and their weighted sum (right).

ions. The agreement between the LFM calculations and the measured Fe $2p$ XAS spectrum is not as good as that for Mn $2p$ XAS [Fig. 1(b)], and the quality of fitting is comparable to each other. Hence, $MnFe_2O_4$ can be described either by $(Mn_{0.8}^{2+}Fe_{0.2}^{3+})_A[Fe_{1.8}^{3+}Mn_{0.2}^{2+}]_BO_4$ or by $(Mn_{0.8}^{2+}Fe_{0.2}^{3+})_A[Fe_{1.6}^{3+}Fe_{0.2}^{2+}Mn_{0.2}^{3+}]_BO_4$.

Figure 3 shows the two Mn $2p$ and Fe $2p$ absorption spectra of $MnFe_2O_4$ for different magnetization directions, which are obtained with the photon helicity parallel to (ρ_+) and antiparallel to (ρ_-) the applied magnetic field. The bottom panels show the XMCD spectra obtained from the difference ($\Delta\rho$) between ρ_+ and ρ_- ($\Delta\rho=\rho_+-\rho_-$) and their integrated values ($\int\Delta\rho$). The spectra of ρ_+ and ρ_- are roughly divided into the L_3 ($2p_{3/2}$) and L_2 ($2p_{1/2}$) regions. According to the sum rule,[15] $\int\Delta\rho$ can be used to estimate the element-specific m_l value.

The Mn $2p$ XMCD is similar to that in the literature.[17,29] This figure reveals the following features. First, the polarity of the Fe $2p$ XMCD is opposite to that of the Mn $2p$ XMCD, which indicates the antiparallel alignment of the spin moments between Fe and Mn ions. This finding is consistent with the ferrimagnetic behavior of $MnFe_2O_4$. Note, however, that this opposite polarity between Mn $2p$ and Fe $2p$ XMCD does not tell whether the ferrimagnetic spin order is collinear or noncollinear. Secondly, the integrated value of the Fe $2p$ XMCD over the whole (L_3+L_2) range, $\int_{L_3+L_2}\Delta\rho$, is finite, while that for the Mn $2p$ XMCD is zero. Since $\int_{L_3+L_2}\Delta\rho$ is proportional m_l,[15] this difference indicates that the orbital moments of Fe ions are not completely quenched in contrast to the quenched orbital moments of Mn ions. The orbital moment should be quenched for Fe^{3+} ions under both O_h and T_d symmetries. Thus, the nonzero m_l of Fe ions might reflect the existence of Fe^{2+} ions at $B(O_h)$ sites, which is favored by the mixed-valent Fe states with a structural formula of $(Mn_{0.8}^{2+}Fe_{0.2}^{3+})_A$ $[Fe_{1.6}^{3+}Fe_{0.2}^{2+}Mn_{0.2}^{3+}]_BO_4$.

Figure 4 compares the Fe $2p$ XMCD spectrum of $MnFe_2O_4$ to those of $GaFeO_3$ (Ref. 23) and γ-Fe_2O_3.[23,28] The weighted sum (black line) of [$GaFeO_3$ (70%) and γ-Fe_2O_3 (30%)] is superposed upon $MnFe_2O_4$. Note that the XMCD spectrum of $GaFeO_3$ has the contribution only from O_h Fe^{3+} ions,[23] whereas that of γ-Fe_2O_3 has a mixture of Fe_A^{3+} (T_d) and Fe_B^{3+} (O_h) ions[28] (see the labels in Fig. 4). In γ-Fe_2O_3, the sign of the dichroic contribution of Fe_A^{3+} (T_d) ions to XMCD is opposite to that of Fe_B^{3+} (O_h) ions because the main magnetic coupling between A and B sites is antiferromagnetic. The good agreement between $MnFe_2O_4$ and the weighted sum of $GaFeO_3$ and γ-Fe_2O_3 indicates the existence of Fe_A^{3+} (T_d) ions in $MnFe_2O_4$ (see the feature around $h\nu\sim708$ eV). Considering 100% O_h Fe^{3+} ions for $GaFeO_3$ and $Fe_A^{3+}/Fe_B^{3+}=T_d/O_h=3/5$ for γ-Fe_2O_3, the fitting yields the estimated T_d/O_h ratio in $MnFe_2O_4$ to be $T_d/O_h=0.11/0.89\approx0.1/0.9$. This value agrees with the estimated inversion parameter of $y\sim0.2$ in Fig. 1 within the experimental error.

The right panel of Fig. 4 compares the Fe $2p$ XMCD spectrum of $MnFe_2O_4$ to the calculated XMCD spectra for Fe_B^{3+} (O_h) (Ref. 28) and Fe_A^{3+} (T_d) (Ref. 28) and their weighted sum (black line) of [Fe_B^{3+} (O_h) (90%) and Fe_A^{3+} (T_d) (10%)]. Here, we have assumed the single-valence state of Fe^{3+} at both $B(O_h)$ and $A(T_d)$ sites. A reasonably good agreement is found between experiment and calculations. Therefore, this comparison supports the inversion of ~10% of Fe ions from $B(O_h)$ sites to $A(T_d)$ sites.

Figure 5 compares the Mn $2p$ XMCD spectrum of $MnFe_2O_4$ to the calculated Mn $2p$ XMCD spectra for different valence states of Mn ions,[30] including $Mn^{2+}(3d^5)$ and $Mn^{3+}(3d^4)$ and their weighted sums of [50% Mn^{2+} and 50% Mn^{3+} and 80% Mn^{2+} and 20% Mn^{3+}. These calculations describe the multiplet features of XMCD of $Mn^{2+}(3d^5)$ and $Mn^{3+}(3d^4)$ qualitatively. In particular, the negative feature (marked with an arrow) around $h\nu\sim641$ eV increases with the increasing $Mn^{3+}(3d^4)$ component.[17] On the other hand, both 100% Mn^{2+} calculation and the sum of 80% Mn^{2+} and 20% Mn^{3+} calculations seem to agree to the measured Mn $2p$

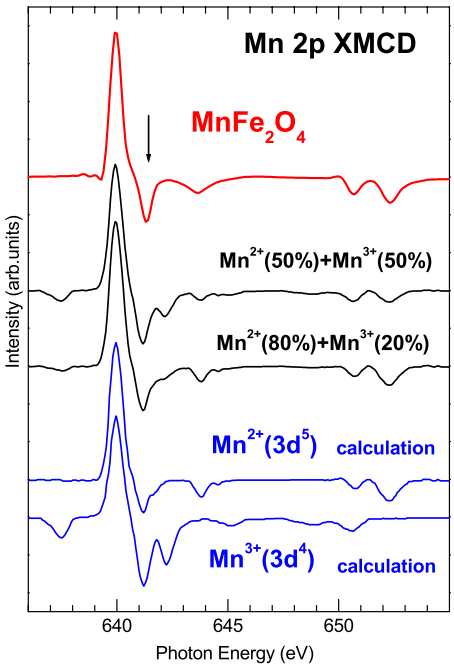

FIG. 5. (Color online) Comparison of the Mn $2p$ XMCD of $MnFe_2O_4$ to the calculated Mn $2p$ XMCD for $Mn^{+}(3d^6)$, $Mn^{2+}(3d^5)$, and $Mn^{3+}(3d^4)$ ions (Ref. 30) and their weighted sums.

XMCD of $MnFe_2O_4$ within the fitting uncertainty. This finding is again in agreement with that of Mn $2p$ XAS (see Fig. 1).

Our XAS/XMCD data indicate that Mn ions are nearly divalent (Mn^{2+}) and that Fe ions are nearly trivalent (Fe^{3+}), with the inversion of $y \sim 0.2$. On the other hand, we cannot determine exactly whether $MnFe_2O_4$ is $(Mn^{2+}_{0.8}Fe^{3+}_{0.2})_A[Fe^{3+}_{1.8}Mn^{2+}_{0.2}]_BO_4$ or $(Mn^{2+}_{0.8}Fe^{3+}_{0.2})_A[Fe^{3+}_{1.6}Fe^{2+}_{0.2}Mn^{3+}_{0.2}]_BO_4$, as explained above. Note that the dominating Fe^{3+} and Mn^{2+} ions in $MnFe_2O_4$ obtained from the present analysis are compatible with the spinel cubic structure of $MnFe_2O_4$ with the negligible JT distortion because both $Fe^{3+}(3d^5)$ and $Mn^{2+}(3d^5)$ ions are not JT active.

Now, we discuss on the reduced magnetic moment in $MnFe_2O_4$. In AB_2O_4-type spinel oxides, the antiferromagnetic coupling between magnetic moments of A and B sites is dominating. Then, in the ionic model, the configuration of $(Mn^{2+}_{0.8}Fe^{3+}_{0.2})_A[Fe^{3+}_{1.8}Mn^{2+}_{0.2}]_BO_4$ for $MnFe_2O_4$ has the magnetic moment of $5\mu_B$/f.u., while $(Mn^{2+}_{0.8}Fe^{3+}_{0.2})_A[Fe^{3+}_{1.6}Fe^{2+}_{0.2}Mn^{3+}_{0.2}]_BO_4$ for $MnFe_2O_4$ has the magnetic moment of $4.6\mu_B$/f.u. The magnetic moment of the latter configuration is consistent with the observed magnetic moment. Nevertheless, one should be cautious because, in solids, the magnetic moment would not be explained simply in terms of the ionic model due to the rather complicated solid-state effects, such as the hybridization effect between T and ligand oxygen ions. Indeed, the existing band-structure calculations[31–34] indicate that the magnetic moments of Mn and Fe ions are reduced a lot from the values predicted by the ionic model. For example, Penicaud *et al.*[31] obtained the magnetic moments of $(2.96-3.96)\mu_B$ for Mn and $(3.29-3.75)\mu_B$ for Fe, which are much smaller than $5.0\mu_B$ of both Mn^{2+} and Fe^{3+} and $4.0\mu_B$ of both Mn^{3+} and Fe^{2+} in the ionic model. The reference oxides employed in Figs. 2 and 4, which are assumed to have the formal integer valences, might also have some mixed configurations of valence states through the hybridization between T and ligand oxygen ions.

In conclusion, the valence and spin states of $MnFe_2O_4$ have been investigated by performing XAS and XMCD measurements near the Mn $2p$ and Fe $2p$ absorption edges. The valence states of Mn and Fe ions are found to be nearly divalent (Mn^{2+}) and trivalent (Fe^{3+}), respectively. The analysis of the XAS and XMCD line shapes provides evidence for the inversion with $y \sim 0.2$. Based on our data, $MnFe_2O_4$ can be described either by $(Mn^{2+}_{0.8}Fe^{3+}_{0.2})_A[Fe^{3+}_{1.8}Mn^{2+}_{0.2}]_BO_4$ or by $(Mn^{2+}_{0.8}Fe^{3+}_{0.2})_A[Fe^{3+}_{1.6}Fe^{2+}_{0.2}Mn^{3+}_{0.2}]_BO_4$. The polarity of the Fe $2p$ XMCD is opposite to that of the Mn $2p$ XMCD, which reveals the antiparallel alignment of the spin moments between Fe and Mn ions. Further, the orbital moments of Fe ions are not completely quenched, while the orbital moments of Mn ions are nearly quenched in $MnFe_2O_4$.

This work was supported by the KRF (KRF-2006-311-C00277), by the KOSEF (R01-2006-000-10369-0), and by the KOSEF through the CSCMR at SNU and the eSSC at POSTECH. B.I.M. also acknowledges the support from POSTECH research fund. The PAL is supported by the MOST and POSCO in Korea.

*kangjs@catholic.ac.kr

[1] C. L. Zhang, S. Yeo, Y. Horibe, Y. J. Choi, S. Guha, M. Croft, and S.-W. Cheong, Appl. Phys. Lett. **90**, 133123 (2007).
[2] J. B. Goodenough, *Magnetism and the Chemical Bond* (Krieger, New York, 1976).
[3] J. M. Hastings and L. M. Corliss, Phys. Rev. **104**, 328 (1956).
[4] Z. Šimša and V. A. M. Brabers, IEEE Trans. Magn. **11**, 1303 (1975).
[5] F. W. Harrison, W. P. Osmond, and R. W. Teale, Phys. Rev. **106**, 865 (1957).
[6] G. A. Sawatzky, F. van der Woode, and A. H. Morrish, Phys. Rev. **187**, 747 (1969).
[7] G. F. Dionne, J. Appl. Phys. **63**, 3777 (1988).
[8] H. Yasuoka, J. Phys. Soc. Jpn. **19**, 1182 (1964).
[9] T. Shirakashi and T. Kubo, Am. Mineral. **64**, 599 (1979).
[10] J. H. Shim, S. Lee, and B. I. Min, Phys. Rev. B **75**, 134406 (2007).
[11] F. M. F. de Groot, J. C. Fuggle, B. T. Thole, and G. A. Sawatzky, Phys. Rev. B **42**, 5459 (1990).
[12] G. van der Laan and I. W. Kirkman, J. Phys.: Condens. Matter **4**, 4189 (1992).
[13] S. C. Wi, J.-S. Kang, J. H. Kim, S.-B. Cho, B. J. Kim, S. Yoon, B.

J. Suh, S. W. Han, K. H. Kim, K. J. Kim, B. S. Kim, H. J. Song, H. J. Shin, J. H. Shim, and B. I. Min, Appl. Phys. Lett. **84**, 4233 (2004).

[14] B. T. Thole, P. Carra, F. Sette, and G. van der Laan, Phys. Rev. Lett. **68**, 1943 (1992).

[15] C. T. Chen, Y. U. Idzerda, H.-J. Lin, N. V. Smith, G. Meigs, E. Chaban, G. H. Ho, E. Pellegrin, and F. Sette, Phys. Rev. Lett. **75**, 152 (1995).

[16] S. Suga and S. Imada, J. Electron Spectrosc. Relat. Phenom. **92**, 1 (1992).

[17] L. Stichauer, A. Mirone, S. Turchini, T. Prosperi, S. Zennaro, N. Zema, F. Lama, R. Pontin, Z. Šimša, Ph. Tailhades, and C. Boningue, J. Appl. Phys. **90**, 2511 (2001).

[18] We performed x-ray diffraction (XRD) measurements several times over a long time, in which the same sharp XRD patterns were observed. This finding reveals that $MnFe_2O_4$ samples are stable at room temperature.

[19] The TEY mode has proving depth of 50–100 Å

[20] Single crystal of $Fe_{0.9}Mn_{2.1}O_4$ was cleaved *in situ* and measured under the same conditions as for $MnFe_2O_4$.

[21] C. Mitra, Z. Hu, P. Raychaudhuri, S. Wirth, S. I. Csiszar, H. H. Hsieh, H.-J. Lin, C. T. Chen, and L. H. Tjeng, Phys. Rev. B **67**, 092404 (2003).

[22] P. Ghigna, A. Campana, A. Lascialfari, A. Caneschi, D. Gatteschi, A. Tagliaferri, and F. Borgatti, Phys. Rev. B **64**, 132413 (2001).

[23] J.-Y. Kim, T. Y. Koo, and J.-H. Park, Phys. Rev. Lett. **96**, 047205 (2006).

[24] T. J. Regan, H. Ohldag, C. Stamm, F. Nolting, J. Lüning, J. Stöhr, and R. L. White, Phys. Rev. B **64**, 214422 (2001).

[25] Hangil Lee *et al.* (unpublished).

[26] J. P. Crocombette, M. Pollak, F. Jollet, N. Thromat, and M. Gautier-Soyer, Phys. Rev. B **52**, 3143 (1995).

[27] A. Mirone, M. Sacchi, and S. Gota, Phys. Rev. B **61**, 13540 (2000).

[28] γ-Fe_2O_3 is often represented by $(Fe^{3+})_A[Fe^{3+}_{5/3}]_BO_4$ spinel with vacancies at *B* sites. S. Brice-Profeta, M.-A. Arrio, E. Tronc, N. Menguy, I. Letard, C. Cartier dit Moulin, M. Nogues, C. Chaneac, J.-P. Jolivet, and Ph. Sainctavit, J. Magn. Magn. Mater. **288**, 354 (2005).

[29] P. Ferriani, G. Ghiringhelli, G. Ferrari, C. M. Bertoni, A. Tagliaferri, L. Braicovich, and N. B. Brookes, Nucl. Instrum. Methods Phys. Res. B **200**, 220 (2003).

[30] A. P. Holm, S. M. Kauzlarich, S. A. Morton, G. dan Waddil, W. E. Pickett, and J. G. Tobin, J. Am. Chem. Soc. **124**, 9894 (2002).

[31] M. Penicaud, B. Siberchicot, C. B. Sommers, and J. Kübler, J. Magn. Magn. Mater. **103**, 212 (1992).

[32] D. J. Singh, M. Gupta, and R. Gupta, Phys. Rev. B **65**, 064432 (2002).

[33] V. N. Antonov, B. N. Harmon, and A. N. Yaresko, Phys. Rev. B **67**, 024417 (2003).

[34] Z. Szotek, W. M. Temmerman, D. Kodderitzsch, A. Svane, L. Petit, and H. Winter, Phys. Rev. B **74**, 174431 (2006).